J. Fluid Mech. (1989), *vol.* 202, *pp.* 577–594
Printed in Great Britain

The effect of geometry on the gravitational instability of a buoyant region of viscous fluid

By JOHN R. LISTER† AND ROSS C. KERR†
Department of Applied Mathematics and Theoretical Physics, University of Cambridge, Silver Street, Cambridge CB3 9EW, UK

(Received 23 December 1987 and in revised form 16 December 1988)

The low-Reynolds-number stability of a region of buoyant fluid surrounded by denser fluid is analysed in two situations. In the first study, the buoyant fluid lies in a thin layer sandwiched between two denser and much deeper layers. The growth rate and wavelength of the most unstable sinusoidal perturbation are calculated and the effects of the viscosity ratios and density differences between the fluids are investigated. It is found that if the buoyant fluid is much less viscous than the overlying fluid then, in quite general circumstances, both the most unstable wavelength and the corresponding growth rate are inversely proportional to the cube root of the viscosity of the buoyant fluid. A physical explanation of this result is given by scaling analysis of the total dissipation. In the second study, the buoyant fluid takes the form of a cylinder rising through a uniform environment. The eigenmodes of small perturbation about this state of motion are found for each axial wavenumber in terms of Fourier series of separable solutions to the Stokes equations. In contrast to the first study, it is found that the most unstable wavelength and growth rate are asymptotically independent of the viscosity of the buoyant fluid when this viscosity is small.

The difference between the results of the two studies is of importance, particularly for geophysical applications in which viscosity ratios are very large. Previous models of linear regions of volcanism at mid-ocean ridges and at island arcs have assumed that results obtained in simple two-layered systems can be generalized to other geometries. The conclusions of these models are discussed in the light of the stability results for a cylindrical (and hence linear) buoyant region.

1. Introduction

When one or more layers of buoyant fluid underlie a layer of relatively dense fluid the system is unstable: any small disturbance to the interface between the layers will grow until the fluid layers have overturned, possibly with some mixing, and light fluid overlies dense fluid. The nature of the overturning depends on the size and geometry of any boundaries, the viscosities and densities of the fluids and the layer depths. The initial vertical motion is dominated by the wavelength of the most unstable perturbation. If the fluids have large viscosities and their horizontal extent is much greater than the vertical structure of the layering, then subsequent evolution of the motion produces an array of rising blobs of buoyant fluid at a spacing determined by this wavelength (Whitehead & Luther 1975). In the geophysical

† Present address: Research School of Earth Sciences, The Australian National University, GPO Box 4, Canberra, ACT 2601, Australia.

literature these buoyant blobs are usually referred to as diapirs and their formation as diapirism (Braunstein & O'Brien 1968) and we shall adopt this convention here.

The regular spacing of diapirs formed by such buoyant instabilities plays an important role in determining the spatial periodicity of several geological features. Salt-dome formations result when a layered salt deposit underlies a sedimentary overburden of greater density (Nettleton 1934); the planform, spacing and timescale of the subsequent diapirism of salt through sediment was predicted by calculations in a simple layered geometry (Selig 1965; Woidt 1978). More recently, buoyant instabilities have been invoked as an explanation of regularly spaced volcanism observed in continental rifting (Mohr & Wood 1976; Bonatti 1985), in Iceland (Sigurdsson & Sparks 1978), in island arcs (Marsh & Carmichael 1974; Marsh 1979) and along mid-ocean ridges (Whitehead, Dick & Schouten 1984; Schouten, Klitgord & Whitehead 1985; Crane 1985). In these cases, it is suggested that a region of buoyant, partially molten material accumulates at depth, that when sufficient material has accumulated a gravitational instability develops, and that the resultant diapirs rapidly carry the buoyant material to the surface. The source regions are left depleted of melt and the cycle then repeats. Measurements of the wavelength and estimates of the timescale of formation of these features have been used to infer values for the properties and dimensions of the relevant regions of mantle. It is essential, therefore, to have an appropriate model for these instabilities.

The early geophysical applications prompted analyses of the linear stability of some specific layered systems (Biot & Odé 1965; Selig 1965; Whitehead & Luther 1975) and numerical simulation of general layered systems (Ramberg 1968*a*, *b*). However, in applications of gravitational-instability models to volcanism at mid-ocean ridges and at island arcs, the linear arrangement of the volcanoes is not consistent with the use of planar geometry; instead it suggests that they arise from underlying magmatic sources that are narrow and linear. Recent experimental work has investigated diapir formation and spacing on a rising cylinder of buoyant fluid and at the leading edge of a rising buoyant sheet (Whitehead *et al.* 1984; Kerr & Lister 1988).

Nevertheless, the lack of a theoretical analysis of instabilities to linear fluid bodies such as a cylinder or sheet has led previous workers to ignore differences in geometry and assume that results from layered systems may be applied to other configurations. The results to be presented show that this assumption is fundamentally incorrect. We describe the theoretical solution of two model problems which highlight the dependence of the spacing and growth rate of diapirs upon the geometry of the buoyant structure giving rise to the instability. In §2 we present a linear stability analysis of a thin buoyant layer of fluid sandwiched between two denser and much deeper layers. Significant differences in behaviour are found between this model and earlier two-layer models. In particular, if the densities of the upper and lower layers of our model are similar then the most unstable wavelength may be very large or even infinite. In §3 we present a stability analysis of a horizontal cylinder of buoyant fluid rising through a uniform environment. The eigenmodes of perturbation are found for each axial wavenumber as Fourier series in the azimuthal dependence of separable solutions to the Stokes equations. The wavelength and growth rate of the most unstable perturbation are then determined numerically. The analytical results are discussed in §4 and are found to be in reasonable agreement with experimental observations. The results from the cylindrical geometry differ greatly, however, from the stability results for a layer when the viscosity of the buoyant fluid is much less than its environment. The geophysical implications are discussed in §5.

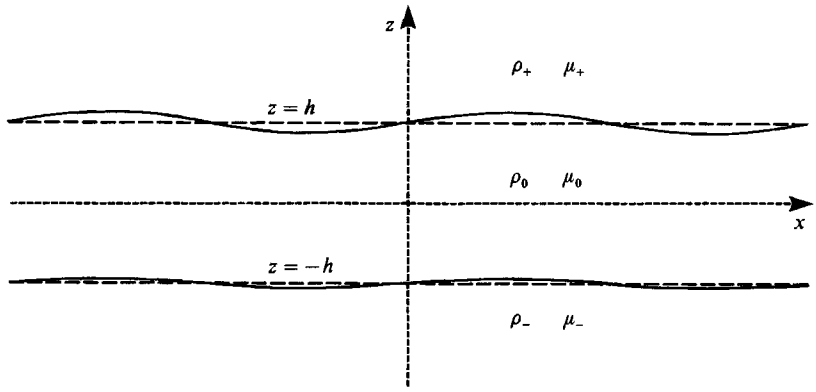

FIGURE 1. Definition sketch. A layer of buoyant fluid is sandwiched between two semi-infinite layers of denser fluids. The interfaces between the layers are given small sinusoidal perturbations from their initial positions at $z = \pm h$.

2. Gravitational instability of a buoyant layer

Consider a layer of buoyant fluid lying in $-h \leqslant z \leqslant h$, sandwiched between two semi-infinite layers of fluid in $h \leqslant z < \infty$ and $-\infty < z \leqslant -h$. Let the viscosities μ and densities ρ of the fluids be as shown in figure 1. Motivated by the extremely large viscosities of geological fluids, we assume that inertial effects are negligible and that the fluid motion is thus governed by the Stokes equations. We also assume that diffusion may be ignored on the timescale of the instability and that surface tension is negligible.

It is convenient to non-dimensionalize lengths with respect to h, times with respect to $\mu_0/((\rho_+ - \rho_0)gh)$, and fluid properties with respect to those of the sandwiched layer, ρ_0 and μ_0. This gives rise to the dimensionless parameters $V = \mu_+/\mu_0$, $W = \mu_-/\mu_0$ and $P = (\rho_- - \rho_0)/(\rho_+ - \rho_0)$ (assumed positive). From now on all variables will be dimensionless unless explicitly stated otherwise.

We look for eigenmodes of the linearized equations of motion corresponding to two-dimensional sinusoidal perturbations of the interface. All quantities may thus be written as $f(z)\,\mathrm{e}^{\mathrm{i}kx+\sigma t}$, where k is the wavenumber and σ the growth rate of the disturbance. The Stokes equations require the stream function ψ to satisfy $\nabla^4\psi = 0$. The boundary conditions of no flow as $z \to \pm\infty$ further reduce ψ to the form

$$\psi_+ = (A + Bz)\,\mathrm{e}^{-zk}\,\mathrm{e}^{\mathrm{i}kx+\sigma t} \qquad (z \geqslant 1), \tag{2.1a}$$

$$\psi_0 = ((C + Dz)\,\mathrm{e}^{-zk} + (E + Fz)\,\mathrm{e}^{zk})\,\mathrm{e}^{\mathrm{i}kx+\sigma t} \qquad (|z| \leqslant 1), \tag{2.1b}$$

$$\psi_- = (G + Hz)\,\mathrm{e}^{zk}\,\mathrm{e}^{\mathrm{i}kx+\sigma t} \qquad (z \leqslant -1). \tag{2.1c}$$

The eight unknown constants, A to H, are determined by the eight linearized boundary conditions arising from continuity of the vertical and horizontal components of velocity and stress at the two interfaces. These boundary conditions take the form

$$\left.\begin{aligned} \psi_+ &= \psi_0 && (2.2a)\\ \mathrm{D}\psi_+ &= \mathrm{D}\psi_0 && (2.2b)\\ V(\mathrm{D}^2 + k^2)\psi_+ &= (\mathrm{D}^2 + k^2)\psi_0 && (2.2c)\\ V(\mathrm{D}^2 - 3k^2)\,\mathrm{D}\psi_+ &= (\mathrm{D}^2 - 3k^2)\,\mathrm{D}\psi_0 + \frac{\psi_0 k^2}{\sigma} && (2.2d) \end{aligned}\right\} \quad (z = 1),$$

$$\left.\begin{aligned} \psi_- &= \psi_0 && (2.2e)\\ \mathrm{D}\psi_- &= \mathrm{D}\psi_0 && (2.2f)\\ W(\mathrm{D}^2+k^2)\psi_- &= (\mathrm{D}^2+k^2)\psi_0 && (2.2g)\\ W(\mathrm{D}^2-3k^2)\,\mathrm{D}\psi_- &= (\mathrm{D}^2-3k^2)\,\mathrm{D}\psi_0+\frac{P\psi_0 k^2}{\sigma} && (2.2h) \end{aligned}\right\} \quad (z=-1),$$

where D denotes $\partial/\partial z$. Substitution from (2.1) into (2.2), followed by elimination of A, B, G and H, yields a linear homogeneous set of four equations for C, D, E and F. After some manipulation, we deduce that a solution is possible provided that

$$\begin{vmatrix} V-1-\dfrac{1}{2k\sigma} & \left(V+1-\dfrac{1}{2k\sigma}\right)\mathrm{e}^{2k} & 0 & 0 \\ (1-V)(2k-1) & (1+V)(2k+1) & -(V+1)\,\mathrm{e}^{2k} & 1-V \\ 0 & 0 & W-1+\dfrac{P}{2k\sigma} & \left(W+1+\dfrac{P}{2k\sigma}\right)\mathrm{e}^{2k} \\ -(W+1)\,\mathrm{e}^{2k} & 1-W & (1-W)(2k-1) & (1+W)(2k+1)\,\mathrm{e}^{2k} \end{vmatrix} = 0. \quad (2.3)$$

Equation (2.3) is a quadratic for the growth rate $\sigma(k;P,V,W)$; the two roots are both real and correspond to the pair of eigenmodes of perturbation for a system with two interfaces. We shall consider throughout the most positive root for σ, that is the least stable root, and will concentrate on three issues: (i) when is there a maximum growth rate σ^* at a finite wavelength $2\pi/k^*$; (ii) if k^* and σ^* exist, then how do they depend on P, V and W; and (iii) what happens as $V, W \to \infty$?

We note that in any real situation $k^* = 0$ will not be achieved, owing either to violation of the assumption of semi-infinite layers, or to the appearance of inertial effects at sufficiently large wavelengths. In such a case, the spacing of the diapirs would be determined by the horizontal extent of the layers, by the finite depths of the upper and lower layers, or by an inertial lengthscale, and would not scale with the depth of the buoyant layer.

2.1. *The existence of a finite optimum wavelength*

It is found that, for given values of P, V and W, σ is either a monotonically decreasing function of k and thus $k^* = 0$; or it has a single maximum at $k^* > 0$. The local behaviour of σ around $k = 0$ can be found by Taylor expansion of the quadratic (2.3).

(*a*) When $P < 1$,

$$\sigma \sim \frac{1-P}{2k(V+W)}, \quad k^* = 0. \quad (2.4)$$

We see that, as expected, when the lower half-space is less dense than the upper the system is very unstable – a balance between buoyancy forces ($\propto k^{-3}$) and viscous drag ($\propto \sigma k^{-2}$) results in a growth rate proportional to k^{-1} as $k \to 0$, in which the thin intermediate layer plays no role.

(*b*) Conversely, when $P > 1$ the lower half-space is more dense than the upper and

$$\sigma \sim \frac{2kP}{(V+W)(P-1)}, \quad k^* > 0 \quad (V+W \neq 0). \quad (2.5)$$

(The root given by (2.4) is now the most stable root and of no interest.) As an

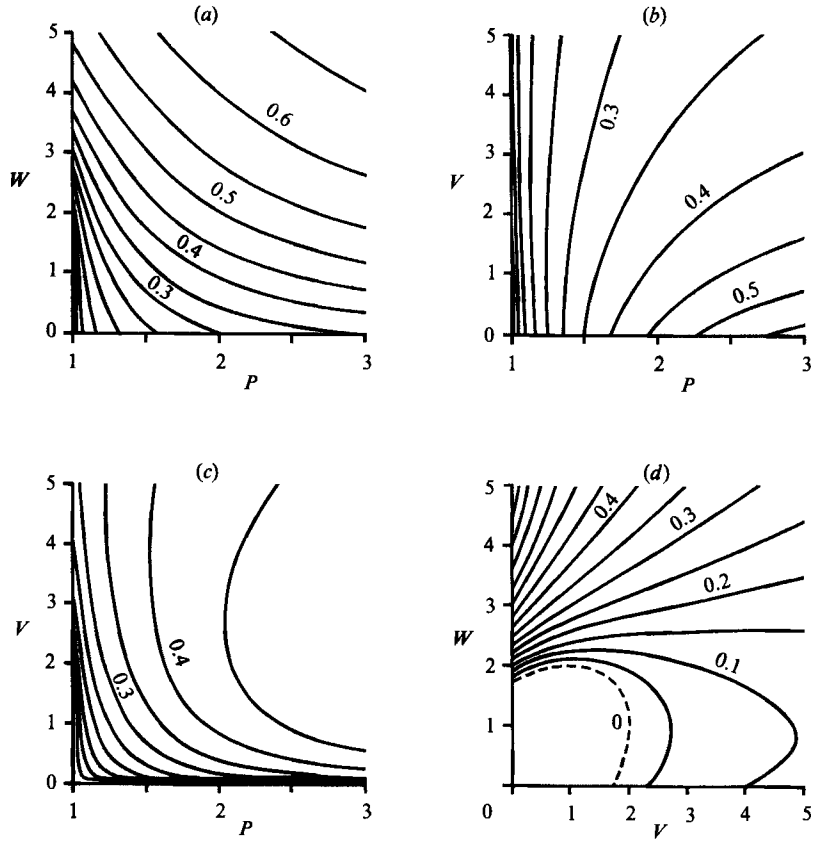

FIGURE 2. Contours of the wavenumber, $k^*(P, V, W)$, of the most unstable disturbance to a buoyant layer, drawn in four cross-sections of (P, V, W)-space: (*a*) $V = 1$; (*b*) $W = 1$; (*c*) $V = W$; and (*d*) $P = 1$ (ellipse (2.6) dashed).

exceptional case of (2.5), we note that if $V = W = 0$ then $\sigma \sim P(1-\frac{16}{45}k^4)/(2(P-1))$ and hence $k^* = 0$. This exception corresponds to comparatively inviscid upper and lower layers, with instability occurring at the wavelength that minimizes deformation of the viscous intermediate layer.

(*c*) Finally, if the upper and lower layers have equal densities ($P = 1$) then it may be shown that $\sigma \sim (1+O(k))/(V+W)$. Inspection of the $O(k)$-term reveals that $k^* = 0$ if

$$12 \geqslant (V+W)^2+3(V-W)^2 \tag{2.6}$$

and $k^* > 0$ otherwise. For the subcase $V = W$, this result shows that the numerical results of Ramberg (1972, table 1) are incorrect for $V \leqslant \sqrt{3}$ since the possibility that $k^* = 0$ was ignored.

In summary, $k^* = 0$ if either $P < 1$ or both $P = 1$ and (2.6) hold.

2.2. *The dependence of k^* and σ^* on P, V and W*

For situations in which $k^* > 0$, the dependence of k^* and σ^* upon P, V and W is best displayed by contour maps of k^* and σ^* on plane cross-sections of (P, V, W)-space. In figures 2 and 3 we show four such contour maps, the cross-sections chosen being: (*a*) equal upper- and intermediate-layer viscosities $V = 1$; (*b*) equal lower- and intermediate-layer viscosities $W = 1$; (*c*) equal upper- and lower-layer viscosities

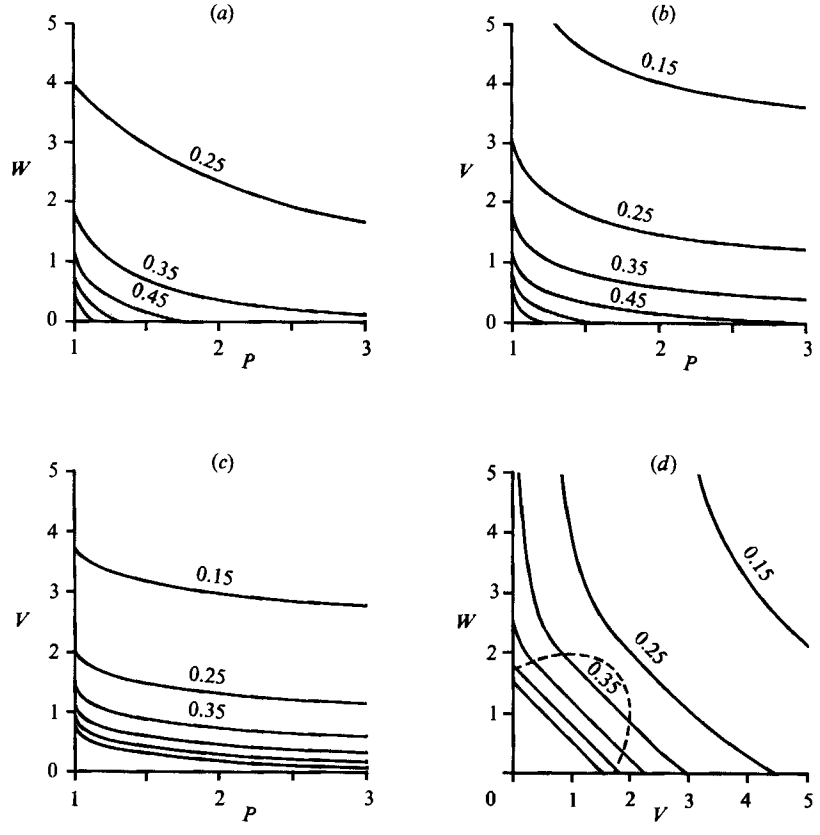

FIGURE 3. Contours of the growth rate, $\sigma^*(k^*; P, V, W)$, of the most unstable disturbance to a buoyant layer, drawn in four cross-sections of (P, V, W)-space: (*a*) $V = 1$; (*b*) $W = 1$; (*c*) $V = W$; and (*d*) $P = 1$ (ellipse (2.6) dashed).

$V = W$; and (*d*) equal upper- and lower-layer densities $P = 1$. In case (*d*) the ellipse defined by (2.6) is shown explicitly; within the ellipse $k^* = 0$ and $\sigma^* = 1/(V+W)$.

As expected, σ^* is seen to be a decreasing function of P, V and W since an increase in the density of the lower layer, or in the viscosities, inhibits motion and retards growth of the instability. The optimal wavenumber k^* is determined by a balance between two conflicting requirements: the ratio of buoyancy to viscous forces is greater the larger the lengthscale of the flow, whereas the ease of moving fluid by half a wavelength from a thinning region in the intermediate layer to a thickening region is greater the smaller the lengthscale of the flow. Increases in either P or in W reflect an increasing difficulty in moving the lower layer and increases the importance of the latter requirement. An increase in V reflects an increase in the viscous forces in the upper layer and in the importance of the former requirement. We would therefore expect k^* to be an increasing function of P and W and a decreasing function of V. This is seen to be the case.

2.3. *The limit of large viscosity ratios*

The three-layer model we have chosen encompasses some previously studied two-layer models as degenerate subcases. Selig (1965) considered a layer of buoyant fluid underlying denser fluid and supported either by a rigid lower boundary or by a free-

slip though non-deformable lower boundary. The analyses are recovered in the limits of $W \to \infty$ and of $P \to \infty, W \to 0$. In the further limit $V \gg 1$ the results are

$$k^* \sim \left(\frac{3}{2V}\right)^{\frac{1}{3}}, \quad \sigma^* \sim \left(\frac{2}{81V^2}\right)^{\frac{1}{3}} \quad \text{(rigid)}, \tag{2.7a}$$

$$k^* \sim \left(\frac{3}{8V}\right)^{\frac{1}{3}}, \quad \sigma^* \sim \left(\frac{8}{81V^2}\right)^{\frac{1}{3}} \quad \text{(free-slip)}. \tag{2.7b}$$

(The first of these expressions is a correction to the often-cited† numerical result from Selig 1965 that $2k^* \sim 2.15V^{-\frac{1}{3}}$.)

We find, however, that the asymptotic dependence of k^* and σ^* on V as $V \to \infty$ is much more general than the previous studies would indicate. Detailed analysis of (2.3) reveals that in the limit $V \to \infty$ this equation reduces to a few simple forms.

(*a*) When $W = CV$, $V \to \infty$, and C is fixed, the leading-order terms satisfy

$$(\tfrac{4}{3}Ck^3V + C + 1)(2k\sigma V)^2 + (\tfrac{4}{3}(P-C)k^3V + P - 1)(2k\sigma V) - \tfrac{4}{3}Pk^3V = 0. \tag{2.8a}$$

(*b*) If $W = CV^{\frac{1}{3}}$, $V \to \infty$, and C is fixed, then

$$(C(k^3V)^{\frac{1}{3}} + \tfrac{1}{4})(2k\sigma V)^2 + (\tfrac{4}{3}Pk^3V(C(k^3V)^{\frac{1}{3}} + 1) + (P-1)(C(k^3V)^{\frac{1}{3}} + \tfrac{1}{4}))(2k\sigma V) - \tfrac{4}{3}Pk^3V(C(k^3V)^{\frac{1}{3}} + 1) = 0. \tag{2.8b}$$

(*c*) The limit $W \gg V \gg 1$ may be evaluated directly or recovered from (2.8*a*) by allowing $C \to \infty$. We obtain

$$(\tfrac{4}{3}k^3V + 1)\,2k\sigma V - \tfrac{4}{3}k^3V = 0 \quad (W \gg V). \tag{2.9a}$$

(*d*) The limit $V^{\frac{1}{3}} \ll W \ll V$ is obtained by putting $C = 0$ in (2.8*a*) or by letting $C \to \infty$ in (2.8*b*):

$$(2k\sigma V)^2 + (\tfrac{4}{3}Pk^3V + P - 1)(2k\sigma V) - \tfrac{4}{3}Pk^3V = 0 \quad (V^{\frac{1}{3}} \ll W \ll V). \tag{2.9b}$$

(*e*) By putting $C = 0$ in (2.8*b*) we find that when $W \ll V^{\frac{1}{3}}$

$$(2k\sigma V)^2 + (\tfrac{16}{3}Pk^3V + P - 1)(2k\sigma V) - \tfrac{16}{3}Pk^3V = 0 \quad (W \ll V^{\frac{1}{3}}). \tag{2.9c}$$

In each of these limits, the natural groupings show that

$$k^* \sim c_1(P, W)\,V^{-\frac{1}{3}}, \quad \sigma^* \sim c_2(P, W)\,V^{-\frac{2}{3}}, \tag{2.10}$$

where the coefficients c_1 and c_2 are functions of P and W, which only depend on W if either $W = O(V^{\frac{1}{3}})$ or $W = O(V)$. Thus, if $W \ll V^{\frac{1}{3}}$ or $V^{\frac{1}{3}} \ll W \ll V$ or $V \ll W$ then $k^*V^{\frac{1}{3}}$ and $\sigma^*V^{\frac{2}{3}}$ are functions only of P. The functions appropriate to the three regimes are shown in figures 4 and 5.

The above results may be interpreted, and their generality of application may be explained, in terms of the following physical arguments (taken in dimensionless form). The vertical velocities at the peaks and troughs of the disturbance are $O(\sigma)$. In the upper fluid, shear of $O(\sigma k)$ due to variations in vertical velocity causes viscous dissipation of $O(V\sigma^2)$ per wavelength. By continuity, the horizontal velocity, u, in the buoyant layer is $O(\sigma k^{-1})$. The dissipation in this layer is thus $O(\sigma^2 k^{-3})$ per wavelength. The dissipation in the lower fluid may be shown not to exceed the dissipation in the other two layers. The dissipation is balanced by release of buoyant

† Whitehead & Luther 1975, Marsh & Carmichael 1974, Marsh 1979, Whitehead *et al.* 1984, Bonatti 1985, Crane 1985, Schouten *et al.* 1985.

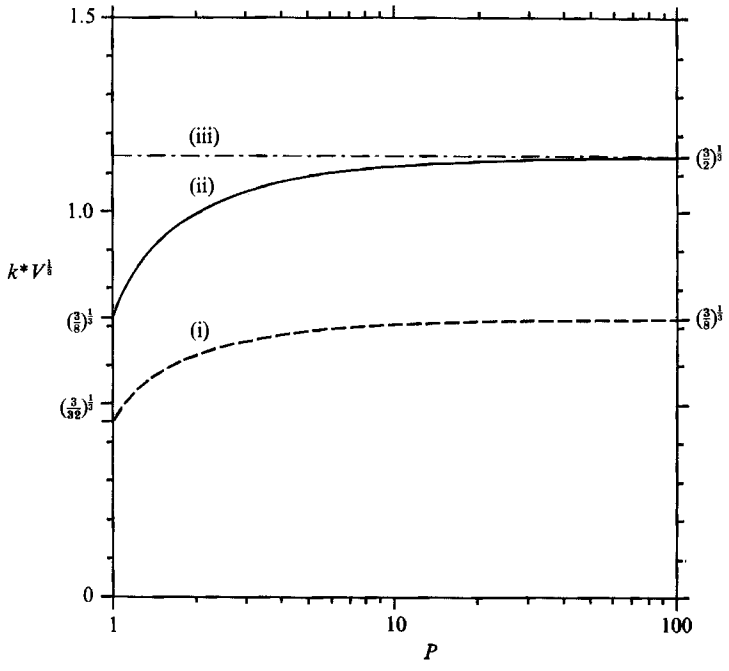

FIGURE 4. The wavenumber of the most unstable disturbance to a buoyant layer in the limit $V \to \infty$: (i) $W \ll V^{\frac{1}{3}}$; (ii) $V^{\frac{1}{3}} \ll W \ll V$; and (iii) $V \ll W$.

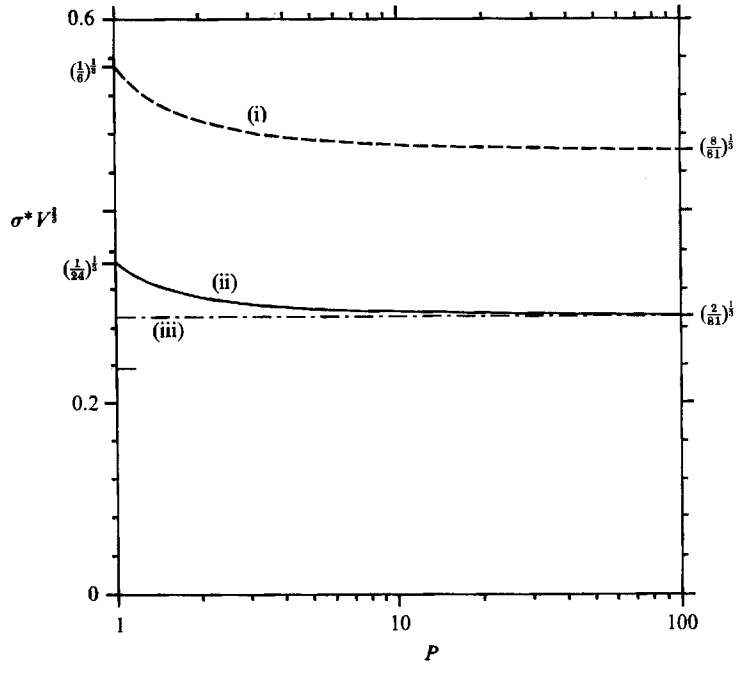

FIGURE 5. The growth rate of the most unstable disturbance to a buoyant layer in the limit $V \to \infty$: (i) $W \ll V^{\frac{1}{3}}$; (ii) $V^{\frac{1}{3}} \ll W \ll V$; and (iii) $V \ll W$.

energy of $O(\sigma k^{-1})$ per wavelength. By seeking the maximum value σ which satisfies the energy balance

$$V\sigma^2 + \sigma^2 k^{-3} \sim \sigma k^{-1} \tag{2.11}$$

we deduce that $\sigma^* \sim V^{-\frac{2}{3}}$ and $k^* \sim V^{-\frac{1}{3}}$, in agreement with our analysis. (Similar energy-balance arguments should prove useful in understanding related problems such as the instability of layers of ferro-fluids under an applied magnetic field (J. E. Wesfreid, personal communication).)

We now consider the effect of the lower layer on disturbances with $k = O(V^{-\frac{1}{3}})$. Suppose that the values at the lower interface of the horizontal velocity and stress in the buoyant layer are of the same order of magnitude as the values averaged over the entire buoyant layer. Then continuity of velocity at the lower interface would suggest that the horizontal velocity in the lower layer is $O(u)$, whereas continuity of stress would suggest that the velocity is $O(uk^{-1}W^{-1})$. We conclude that if $W \gg k^{-1} = O(V^{\frac{1}{3}})$ then the horizontal velocity at the lower interface is much less than the mean velocity in the middle layer and the lower interface appears rigid. Conversely, if $W \ll k^{-1} = O(V^{\frac{1}{3}})$, the horizontal flow has a maximum near the lower interface, the stress there is much less than in the interior of the middle layer, and the lower interface appears free-slip.

The horizontal motion in the intermediate layer causes an accumulation of buoyant fluid at the peaks of the disturbance. The resultant vertical forces cause motion in the upper layer. If $W \ll V$ the buoyancy force must be balanced by the viscous resistance of the upper layer and the lower interface appears perfectly flexible. If $W \gg V$ (or if $P \gg 1$) then the lower interface is effectively non-deformable.

These observations effectively explain the various limits in (2.8) and (2.9). The transition from (2.9*c*) through (2.8*b*) to (2.9*b*) at $W = O(V^{\frac{1}{3}})$ is due to the change from a free-slip lower interface when $W \ll V^{\frac{1}{3}}$ to a no-slip interface when $W \gg V^{\frac{1}{3}}$. The transition from (2.9*b*) through (2.8*a*) to (2.9*a*) at $W = O(V)$ is due to the change from a flexible lower interface when $W \ll V$ to a non-deformable interface when $W \gg V$. If the lower interface is non-deformable then the density of the lower layer is irrelevant and hence (2.9*a*) does not depend on P.

3. Gravitational instability of a buoyant cylinder

Consider a cylinder of buoyant fluid, radius a, initially horizontal and rising with vertical velocity U (to be determined) through an unbounded volume of relatively dense fluid. Let the viscosities and densities of the fluid be as shown in figure 6. We use cylindrical coordinates in the frame in which the cylinder is at rest with the undisturbed interface at $r = a$. As in §2, we describe a linear stability analysis of the basic state, neglecting inertial effects, diffusion and surface tension.

At the outset we non-dimensionalize lengths with respect to the radius a, velocities with respect to $g(\rho_+ - \rho_0)\, a^2/\mu_+$ and fluid properties with respect to those of the external fluid, μ_+ and ρ_+. The resultant dimensionless parameters are the viscosity ratio $V = \mu_+/\mu_0$, the Reynolds number $R = \rho_+ Ua/\mu_+$, and the dimensionless rise velocity

$$\hat{U} = \frac{U\mu_+}{g(\rho_+ - \rho_0)\, a^2}. \tag{3.1}$$

The derivation of the basic flow will be sketched only briefly. We assume that $R \ll 1$. The flow around the cylinder is described by Stokes equations for $r \ll R^{-1}$, but it is necessary to add on the Oseen correction for $r = O(R^{-1})$. Solution of

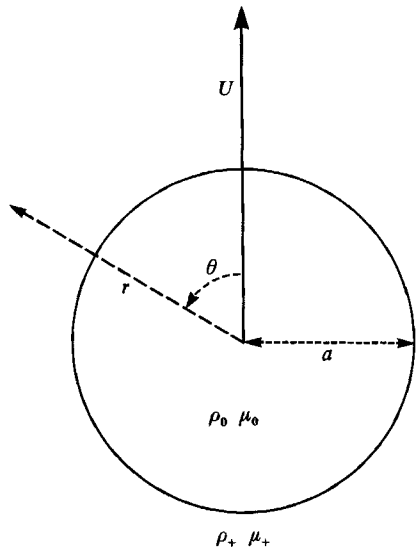

FIGURE 6. Definition sketch. A horizontal cylinder of buoyant fluid, radius a, rises with velocity U through an unbounded viscous fluid.

the equations of motion subject to continuity of velocity and of tangential stress at $r = 1$ yields the following equations for the basic flow field $\boldsymbol{u}^0$:

$$u_r^0 = \frac{V}{8(1+V)}(1-r^2)\cos\theta \qquad (r \leqslant 1); \tag{3.2a}$$

$$u_r^0 = \frac{V}{8(1+V)}\left(\frac{1}{V}\left(1-\frac{1}{r^2}\right)-2\left(1+\frac{1}{V}\right)\ln r\right)\cos\theta \qquad (1 \leqslant r \ll R^{-1}); \tag{3.2b}$$

$$u_\theta^0 = \frac{V}{8(1+V)}(3r^2-1)\sin\theta \qquad (r \leqslant 1); \tag{3.2c}$$

$$u_\theta^0 = \frac{V}{8(1+V)}\left(\frac{1}{V}\left(1-\frac{1}{r^2}\right)+2+2\left(1+\frac{1}{V}\right)\ln r\right)\sin\theta \qquad (1 \leqslant r \ll R^{-1}). \tag{3.2d}$$

By matching to the outer Oseen-flow expansion, we find that U is given implicitly by

$$\hat{U} = \frac{1}{4(V+1)}\left((V+1)\left(\ln\frac{4}{R}-\gamma\right)+V+\tfrac{1}{2}\right)(1+O(\ln R)^{-2}), \tag{3.3}$$

where γ denotes Euler's constant, 0.5772.... A description of the matching technique for the case $V = 0$ may be found in Van Dyke (1964).

We now allow a small perturbation to the interface of the form

$$r = 1+\epsilon f(\theta)\cos kz\, e^{\sigma t}.$$

This induces a perturbation velocity field

$$\boldsymbol{u}^1 = \epsilon(u_r^1(r,\theta)\cos kz, u_\theta^1(r,\theta)\cos kz, u_z^1(r,\theta)\sin kz)\, e^{\sigma t}. \tag{3.4}$$

The linearized boundary conditions for continuity of the three components of velocity and stress may be written in the form

$$[u_r^1]_-^+ = 0, \quad \left[u_\theta^1 + f\frac{\partial u_\theta^0}{\partial r}\right]_-^+ = 0, \quad [u_z^1]_-^+ = 0, \tag{3.5a–c}$$

$$\left[\sigma_{rr}^1 + f\frac{\partial \sigma_{rr}^0}{\partial r}\right]_-^+ = -f\cos\theta, \tag{3.5d}$$

$$\left[\sigma_{r\theta}^1 + f'(\sigma_{rr}^0 - \sigma_{\theta\theta}^0) + f\frac{\partial \sigma_{r\theta}^0}{\partial r}\right]_-^+ = 0, \tag{3.5e}$$

$$[\sigma_{rz}^1 - kf\sigma_{rr}^0]_-^+ = 0, \tag{3.5f}$$

where $[\ ]_-^+$ denotes the difference in values between $r = 1_+$ and $r = 1_-$. The kinematic boundary condition for the motion of the interface is given by

$$\sigma f = u_r^1 + f\frac{\partial u_r^0}{\partial r} - f' u_\theta^0. \tag{3.6}$$

If $R \ll k$ then the perturbation velocity field $\boldsymbol{u}^1$ is given by solving Stokes equations subject to $\boldsymbol{u}^1 \to 0$ as $r \to \infty$ and the boundary conditions (3.5). This serves to establish a linear relation between $\boldsymbol{u}^1$ and f. If we define a linear operator L such that

$$\mathrm{L}f \equiv u_r^1 + f\left(\frac{\partial u_r^0}{\partial r}\right) - f' u_\theta^0$$

then substitution into (3.6) shows that σ is an eigenvalue and f the corresponding eigenfunction of the operator L. We find a representation of L by looking for a Fourier series solution to (3.5) and (3.6).

First, consider the problem

$$\begin{bmatrix} u_r^1 \\ u_\theta^1 \\ u_z^1 \\ \sigma_{rr}^1 \\ \sigma_{r\theta}^1 \\ \sigma_{rz}^1 \end{bmatrix}_-^+ = \begin{Bmatrix} b_1^{(m)}\cos m\theta \\ b_2^{(m)}\sin m\theta \\ b_3^{(m)}\cos m\theta \\ b_4^{(m)}\cos m\theta \\ b_5^{(m)}\sin m\theta \\ b_6^{(m)}\cos m\theta \end{Bmatrix}, \tag{3.7a}$$

$$\mu\nabla^2\boldsymbol{u}^1 = \nabla p^1, \quad \nabla\cdot\boldsymbol{u}^1 = 0. \tag{3.7b,c}$$

We note that if Φ, ψ and $\boldsymbol{A}$ are harmonic functions then

$$\boldsymbol{u}^1 = \nabla\Phi + \boldsymbol{x}\wedge\nabla\psi + \nabla(\boldsymbol{x}\cdot\boldsymbol{A}) - 2\boldsymbol{A}, \quad p^1 = 2\mu\nabla\cdot\boldsymbol{A} \tag{3.8a,b}$$

satisfy (3.7*b*, *c*). Solutions with the appropriate θ-dependence and behaviour at the origin and infinity may be found by taking

$$\psi = 0, \tag{3.9a}$$

$$\Phi = a_1^{(m)}\mathrm{I}_m(kr)\cos kz\cos m\theta \quad (r \leqslant 1), \tag{3.9b}$$

$$\Phi = a_4^{(m)}\mathrm{K}_m(kr)\cos kz\cos m\theta \quad (r \geqslant 1), \tag{3.9c}$$

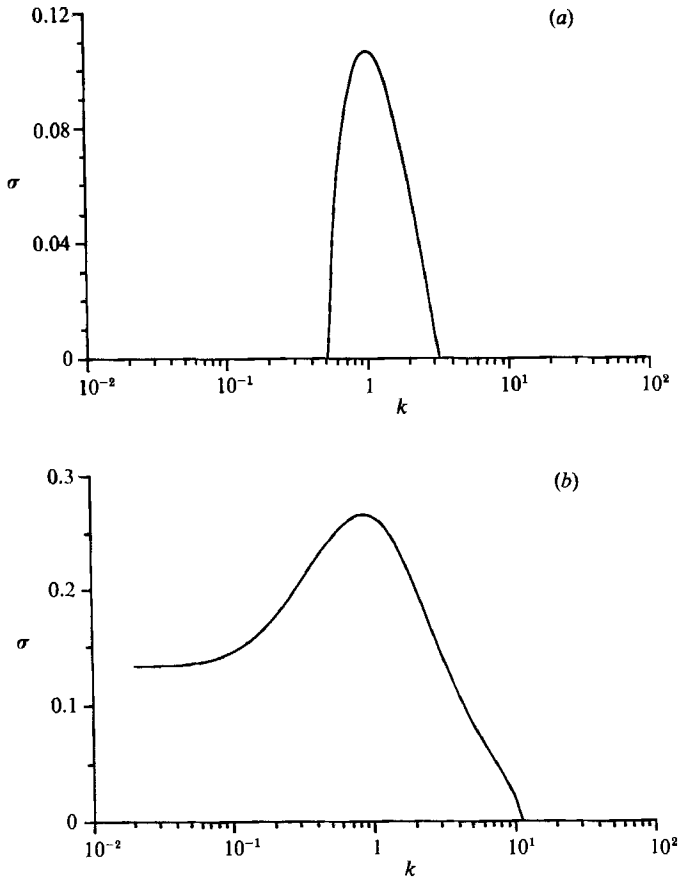

FIGURE 7. The growth rate of disturbances to a buoyant cylinder of fluid as a function of the axial wavenumber, k: (*a*) $V = 1$ and (*b*) $V = 5$.

$$\boldsymbol{A} = ([a_2^{(m)}\mathrm{I}_{m+1}(kr) + a_3^{(m)}\mathrm{I}_{m-1}(kr)]\cos m\theta,$$
$$[a_2^{(m)}\mathrm{I}_{m+1}(kr) - a_3^{(m)}\mathrm{I}_{m-1}(kr)]\sin m\theta, 0)\cos kz \quad (r \leqslant 1), \quad (3.9d)$$
$$\boldsymbol{A} = ([a_5^{(m)}\mathrm{K}_{m+1}(kr) + a_6^{(m)}\mathrm{K}_{m-1}(kr)]\cos m\theta,$$
$$[a_5^{(m)}\mathrm{K}_{m+1}(kr) - a_6^{(m)}\mathrm{K}_{m-1}(kr)]\sin m\theta, 0)\cos kz \quad (r \geqslant 1), \quad (3.9e)$$

where I_m and K_m are modified Bessel functions of order m. Substitution of (3.9) into (3.8) and (3.7) yields six linear equations for the coefficients $a_i^{(m)}, i = 1 \ldots 6$. By inverting these equations, we obtain an expression for $u_r^1(1)$ as a linear combination of $b_i^{(m)}, i = 1 \ldots 6$.

Next, we expand f in a Fourier cosine series with coefficients $f^{(m)}$ and substitute into (3.5). Each Fourier component gives rise to a problem of the form (3.7), in which each $b_i^{(m)}$ is a linear combination of $f^{(m-1)}$ and $f^{(m+1)}$. Solution for $u_r^1(1)$ and substitution into (3.6) yields the eigenvalue equation

$$\mathrm{L}f \equiv \sum_{m=0}^{\infty}\left(\sum_{n=0}^{\infty} A_{mn}(k;V)f^{(n)}\right)\cos m\theta = \sigma \sum_{m=0}^{\infty} f^{(m)}\cos m\theta. \quad (3.10)$$

The matrix A_{mn} is bidiagonal and satisfies $A_{mn} = 0$ if $|m-n| \neq 1$. Despite the banded nature of $\boldsymbol{A}$, it is not possible to determine the eigenvalues σ analytically

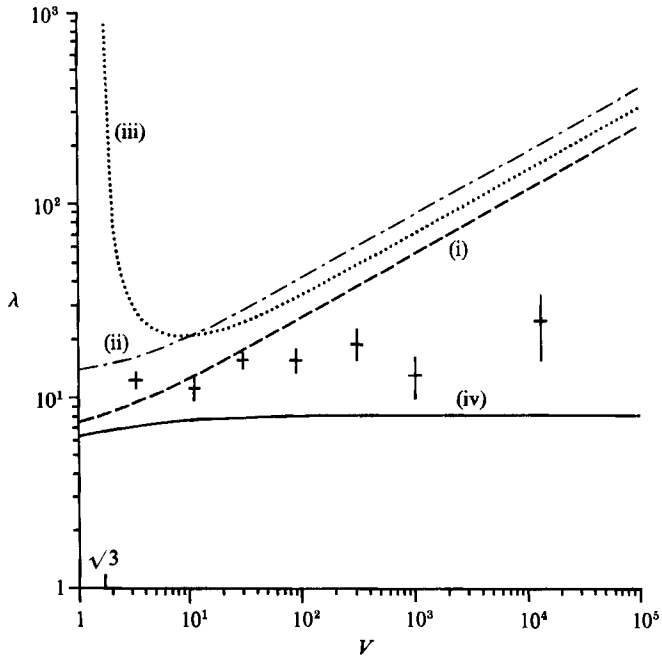

FIGURE 8. The wavelength of the most unstable perturbation to several buoyant structures as a function of the viscosity ratio: (i) two-layer, rigid boundary; (ii) two-layer, free-slip boundary; (iii) three-layer, equal upper and lower properties; (iv) theoretical predictions for a cylinder; and symbols show experimental observations of a cylinder with approximate error bars. (Based on Kerr & Lister 1988, figure 5.)

owing to the complexity of the non-zero elements. Progress can be made by truncation of the Fourier expansion after M terms. The M eigenvalues, $\sigma_i^{(M)}, i = 1, 2, \ldots, M$ of the upper left $M \times M$ corner of $\boldsymbol{A}$ are then determined numerically. If the eigenvectors of $\boldsymbol{A}$ are dominated by low-order Fourier components then we would expect $\{\sigma_i^{(M)}\}$ to tend to the eigenvalues of $\boldsymbol{A}$ as $M \to \infty$. This is found to be the case. The eigenvalues of each truncation are either real or pure imaginary. If the eigenvalues of each truncated matrix are ordered by decreasing real part, and then by increasing imaginary part, then each sequence $\{\sigma_i^{(i)}, \sigma_i^{(i+1)}, \sigma_i^{(i+2)} \ldots\}$ converges to a limit σ_i; the corresponding sequence of eigenvectors is also convergent with the proportion of higher-frequency Fourier components increasing with i. The eigenvalues corresponding to large values of i have large imaginary parts and represent the advection of ripples in the interface by the basic flow. The stability of the basic flow is determined by whether σ_1 is real and positive or imaginary.

Numerical results show that for each V, $\mathrm{Re}(\sigma_1)$ possesses a single (positive) maximum $\sigma^*(V)$ at a wavenumber $k = k^*(V)$. The basic flow is thus always unstable. The range of wavenumbers around k^*, for which $\mathrm{Re}(\sigma_1) > 0$, may be finite or unbounded, depending on the value of V. Typical results are shown in figure 7. The dependence of σ^* and k^* on V will be discussed in the next section.

4. Comparison of results

The models described in §§2 and 3 provide good test cases for questioning some assumptions made in previous models of buoyant instabilities in geophysics. In order

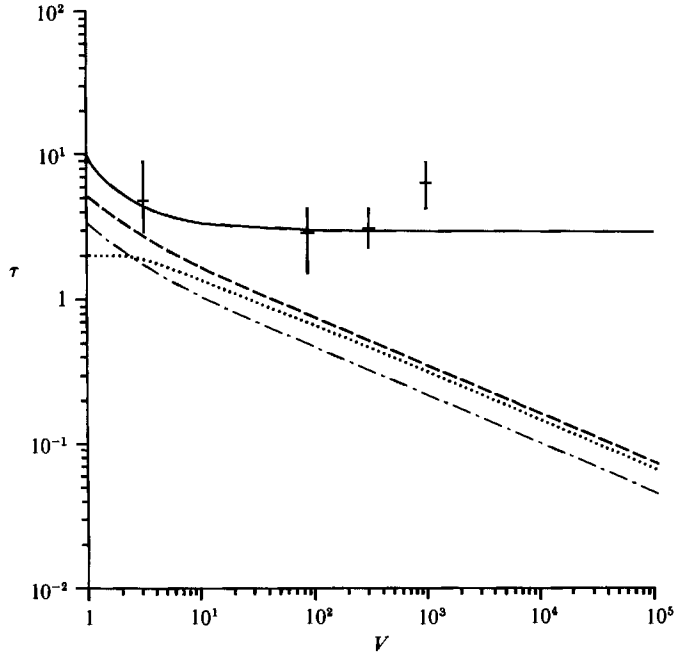

FIGURE 9. The timescale of the maximum growth rate of instabilities of the buoyant structures described in figure 8 as a function of the viscosity ratio.

to compare the results of §2 with those of §3 and of previous workers, we rescale the results of that section by choosing a timescale $\mu_+/((\rho_+-\rho_-)gh)$ based on the viscosity of the upper layer, rather than on the viscosity of the intermediate layer. In figures 8 and 9 (reproduced from Kerr & Lister 1988) we show the dimensionless wavelength, $\lambda = 2\pi/k^*$, and timescale, $\tau = 1/\sigma^*$, of the most unstable perturbation in three examples drawn from §2: (i) a two-layer model with rigid lower boundary ($W = \infty$); (ii) a two-layer model with free-slip, non-deformable lower boundary ($P = \infty$, $W = 0$); and (iii) the case of equal upper- and lower-layer properties ($P = 1, W = V$). In the same diagrams we show the results derived from the theoretical investigation of instabilities to a buoyant cylinder as set out in §3.

Also shown in these figures are measurements of diapir spacing and growth rate for an unstable buoyant cylinder from experiments reported in detail by Kerr & Lister (1988). In these experiments a steady source of relatively buoyant fluid was towed across the interior of a large tank filled with another viscous fluid to produce a trailing cylinder of buoyant fluid which was horizontal and nearly uniform in diameter. This cylinder subsequently rose through the tank and became unstable to asymmetric disturbances; the disturbances rapidly became much larger than the diameter of the cylinder and focused the buoyant fluid into regularly spaced creeping plumes (figure 10). As discussed in Kerr & Lister (1988), the experimental measurements are in reasonable agreement with the theoretical calculations for a cylinder and are clearly incompatible with the predictions from the three layered geometries. We also note here that the cylinder was observed to rise through many times its own diameter before showing signs of instability. This phenomenon may be explained from (3.3) which shows that the dimensionless rise velocity $\hat{U}$ is much larger than σ when $R \ll 1$.

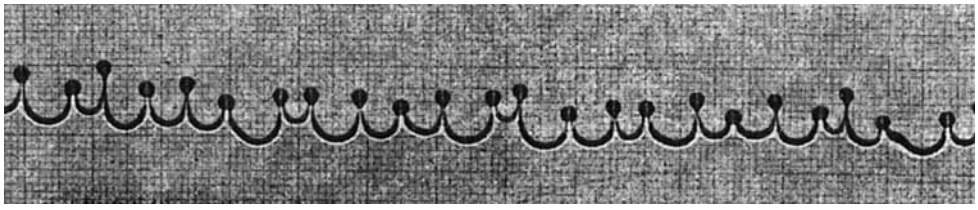

FIGURE 10. Regularly spaced creeping plumes formed by the gravitational instability of a buoyant cylinder ($V = 11$, $a = 0.056$ cm, $\mu_+ = 12.1\,\mathrm{g\,cm^{-1}\,s^{-1}}$, $\rho_+ - \rho_0 = 0.0337\,\mathrm{g\,cm^{-3}}$). The graph paper background has a 1 mm grid. (Reproduced from Kerr & Lister 1988, figure 1.)

The two-layer models, originally described by Selig (1965), give very similar results to each other. The asymptotic dependence of λ and τ on $V = \mu_+/\mu_0$ as $V \to \infty$, namely

$$\lambda \propto V^{\frac{1}{3}}, \quad \tau \propto V^{-\frac{1}{3}}, \tag{4.1a,b}$$

provides a good approximation even when V is not large; the change from a free-slip to a rigid lower boundary gives rise to only a small change in the multiplicative constant. The similarity of the results has led authors writing subsequently to the original studies to suppose that other buoyant instabilities will have a similar dependence on V, with only a slight change in the multiplicative constant (Marsh & Carmichael 1974; Marsh 1979; Whitehead *et al.* 1984; Schouten *et al.* 1985; Crane 1985). Our results show that there is little truth in this assumption and that the geometry of the buoyant region is far more important than had previously been realized.

The results of §2 and the physical arguments given at the end of that section indicate that for a *layered* geometry, the *asymptotic* dependence of λ and τ on V is indeed given by a $V^{\frac{1}{3}}$-relationship. The behaviour at small viscosity ratios, however, may be very different. For example, if the upper and lower layers of a three-layered system have equal densities and the viscosity ratios, V and W, lie within the ellipse defined by (2.6) then $\lambda = \infty$. In this case, as discussed in §2, the spacing of the diapirs would not, in reality, scale with the depth of the buoyant layer.

The contrast between the two-layer results and the cylindrical results is still more striking. Our theoretical analysis of the instability of a cylinder predicts that both λ and τ are asymptotically independent of V as $V \to \infty$:

$$\lambda \sim 8.09\ldots, \quad \tau \sim 2.92\ldots. \tag{4.2a,b}$$

These results are related to the fact that, unlike in the layered geometry, the buoyant region can deform without transport along the axis of the cylinder. The dissipation is thus dominated by the external flow *around* the cylinder.

To sum up, we have shown that the introduction of a deformable lower layer can have a dramatic effect on the predictions of layered models at low viscosity ratios. Further, wavelengths and growth rates of instabilities in layered and cylindrical buoyant structures are seen to be very different at large viscosity ratios. These distinctions have important geophysical implications which will be discussed in the next section.

5. Discussion

In this section we discuss the implications of our results for geophysical modelling. A general point to note is that the stability analyses described in §§2 and 3 are for fixed geometries and are not strictly applicable to geophysical problems in which the geometry evolves with time. An adaptation of the 'frozen-time' treatment of a growing thermal boundary layer (Lick 1965; Howard 1966) allows a connection to be made between σ and the rate at which the geometry is evolving. In the original problem this treatment considers the stability of an instantaneous temperature profile rather than that of the real temperature profile which evolves with time. The method has been found to give good results in Rayleigh–Bénard and Marangoni convection problems (Currie 1967; Vidal & Acrivos 1968). Here we might wish to consider either a buoyant layer underlying a dense layer whose thickness H increases with time (salt-dome formation during deposition of the overburden) or a growing cylindrical region of buoyant fluid (melt generation at island arcs and at mid-ocean ridges). When the overburden or growing cylinder is thin ($H \approx 0$ or $a \approx 0$) the growth rate of the instability is small (equation (4.1*b*) or (4.2*b*)) and much less than the inverse timescale of growth ($\dot{H}/H$ or $\dot{a}/a$). No instability is able to grow in less than the timescale for growth and none of the unstable wavelengths dominates the others since the most unstable wavelength at one time is superseded by a different and more unstable wavelength at later times. As the thickness increases, however, the rate at which the most unstable wavelength is varying due to evolving geometry decreases, while the growth rate τ^{-1} of instability increases. At a well-defined time and thickness the two rates become equal and it is at approximately this time that the instability becomes apparent, grows to large amplitude and drains the buoyant material away in ascending diapirs. It is clear that the buoyant region could not be stabilized by the changing geometry much later than this time since the timescale for instability would be much less than the timescale for changes in geometry. The usefulness of this argument is due to the narrowness of the interval in which the two timescales are of comparable magnitude.

The preceding discussion may be applied to salt-dome formation. If the deposition of the overburden is rapid compared with the timescale of diapirism then the spacing of the diapirs will be given by the most unstable wavelength based on the stratigraphy after deposition. In some regions, however, the observed spacing would appear to be related to the stratigraphy at an intermediate stage of deposition (Craig & Jackson 1987). This may be understood if it is hypothesized that deposition and diapirism occurred synchronously (rather than sequentially) with the spacing 'locked-in' at the most unstable wavelength pertaining when diapirism became dominant. This hypothesis may be tested for consistency since, as described above, the locking-in time may be determined by equating the typical depositional timescale with the instability timescale at locking-in.

For island arc and mid-ocean ridge volcanism, on the other hand, we can equate the instability timescale τ with the timescale for the growth of the buoyant region $a/\dot{a}$ to deduce that

$$\dot{a}_c = \left(\frac{g\,\Delta\rho}{\mu_+}\right) a_c^2, \tag{5.1}$$

where a_c is the critical ribbon radius. If we relate the mean volume flux Q of erupted material to the melt-production rate $2\pi a\dot{a}$ and use (4.2*a*) we obtain

$$Q \propto \left(\frac{g\,\Delta\rho}{\mu_+}\right) \lambda_v^3, \tag{5.2}$$

where λ_v is the typical spacing between volcanoes. The linear relation between Q and λ_v^3 agrees with observations of mid-ocean ridge volcanism (Schouten *et al.* 1985). Since Q and λ_v are observable then we may regard (5.2) as an equation for $\Delta\rho/\mu_+$.

Equation (5.2) depends on the melt fraction c principally through the empirical relationship $\Delta\rho\,(\mathrm{g\,cm^{-3}}) = 0.4c$. In the calculations of Schouten *et al.* (1985), however, the equivalent equation to (5.2) has an extra factor $V^{-\frac{2}{3}}$ on the right-hand side due to its derivation from (4.1) (representing a layered geometry) rather than from (4.2). Large values of c correspond to very large values of V (values in the range 10^4–10^9 would not be unreasonable), so this extra factor would argue against large melt fractions in a layered geometry, since they would lead to inadequate melt-production rates. In contrast, calculations based on (4.2) and (5.2) (derived from an appropriately linear geometry) predict realistic melt-production rates from a region that may be slightly, substantially, or even completely molten (Kerr & Lister 1988).

Our final comment relates to salt-dome formation and to the importance of the properties of the rock underlying the buoyant stratum. This simple observation, whose significance appears not to have been realized, is drawn from our test model of §2. If a buoyant salt deposit overlies an effectively rigid igneous basement then the two-layer models of Selig (1965) may give reasonable results. However, in regions of episodic deposition the salt may overlie the same deformable sediment that forms the overburden. At small viscosity contrasts the dominant wavelength of instability would then be very large and would scale on the depth of the entire deformable region rather than on the thickness of the salt stratum. In this connection, we note the criteria given at the end of §2 for the underlying stratum to be deformable or non-deformable and free-slip or no-slip.

In conclusion, though the stability analysis of general, layered, viscous systems is relatively easy to formalize, in much of the geological literature there seems no clear physical understanding of many of the results. Further, we have shown that the prediction of models of geophysical phenomena need to be treated with caution if they are based on the assumption of a particular geometry. For example, if a buoyant-instability model with a linear, rather than planar, geometry is adopted for island arcs and mid-ocean ridges then the asymptotic dependence of λ and τ on $V^{\frac{1}{3}}$ is removed. As a consequence, previous arguments that the melt fraction is small would have to be abandoned. More generally, we believe that paradigm theoretical studies such as those described here can and should serve as essential guides in clarifying the assumptions of detailed geophysical models.

We would like to thank H. E. Huppert and M. G. Worster for their constructive comments. Financial support from the Natural Environment Research Council and Trinity College, Cambridge (J.R.L.) and from the Royal Commission for the Exhibition of 1851, and Churchill College, Cambridge (R. C. K.) is gratefully acknowledged.

REFERENCES

Biot, M. A. & Odé, H. 1965 Theory of gravitational instability with variable overburden and compaction. *Geophys.* **30**, 213–227.

Bonatti, E. 1985 Punctiform initiation of seafloor spreading in the Red Sea during transition from a continental to an oceanic rift. *Nature* **316**, 33–37.

Braunstein, J. & O'Brien, G. D. 1968 *Diapirism and Diapirs*. Am. Assoc. Petrol. Geol., Mem. 8. 444 pp.

Craig, C. & Jackson, M. P. A. 1987 The spacing of salt diapirs in the Great Kavir: modelling the Rayleigh–Taylor instability with two buoyant layers. *Terra Cognita* **7**, 199.

CRANE, K. 1985 The spacing of rift axis highs: dependence upon diapiric processes in the underlying asthenosphere? *Earth Planet Sci. Lett.* **72**, 405–414.

CURRIE, I. G. 1967 The effect of heating rate on the stability of stationary fluids. *J. Fluid Mech.* **29**, 337–347.

HOWARD, L. N. 1966 Convection at high Rayleigh number. In *Proc. 11th Intl Congr. Appl. Mech., Munich*, pp. 1109–1115. Springer.

KERR, R. C. & LISTER, J. R. 1988 Island arc and mid-ocean ridge volcanism, modelled by diapirism from linear source regions. *Earth Planet. Sci. Lett.* **88**, 143–152.

LICK, W. 1965 The instability of a fluid layer with time dependent heating. *J. Fluid Mech.* **21**, 565–576.

MARSH, B. D. 1979 Island arc development: Some observations, experiments and speculations. *J. Geol.* **87**, 687–713.

MARSH, B. D. & CARMICHAEL, I. S. E. 1974 Benioff zone magmatism. *J. Geophys. Res.* **79**, 1196–1206.

MOHR, P. A. & WOOD, C. A. 1976 Volcano spacing and lithospheric attenuation in the eastern rift of Africa. *Earth Planet. Sci. Lett.* **33**, 126–144.

NETTLETON, L. L. 1934 Fluid mechanics of salt domes. *Bull. Am. Assoc. Petrol. Geol.* **18**, 175–204.

RAMBERG, H. 1968*a* Fluid dynamics of layered systems in a field of gravity, a theoretical basis for certain global structures and isostatic adjustment. *Phys. Earth Planet. Inter.* **1**, 63–87.

RAMBERG, H. 1968*b* Instability of layered systems in a field of gravity, 1, 2. *Phys. Earth Planet. Inter.* **1**, 427–474.

RAMBERG, H. 1972 Mantle diapirism and its tectonic and magmatic consequences. *Phys. Earth Planet. Inter.* **5**, 45–60.

SCHOUTEN, H., KLITGORD, K. D. & WHITEHEAD, J. A. 1985 Segmentation of mid-ocean ridges. *Nature* **317**, 225–229.

SELIG, F. 1965 A theoretical prediction of salt dome patterns. *Geophys.* **30**, 633–643.

SIGURDSSON, H. & SPARKS, R. S. J. 1978 Lateral magma flow within rifted Icelandic crust. *Nature* **274**, 126–130.

VAN DYKE, M. 1964 *Perturbation Methods in Fluid Mechanics*. Academic.

VIDAL, A. & ACRIVOS, A. 1968 Effects of non-linear temperature profiles on the onset of convection driven by surface tension gradients. *Indust. Engng Chem. Fund.* **7**, 53–58.

WHITEHEAD, J. A., DICK, H. B. J. & SCHOUTEN, H. 1984 A mechanism for magmatic accretion under spreading centers. *Nature* **312**, 146–148.

WHITEHEAD, J. A. & LUTHER, D. S. 1975 Dynamics of laboratory diapir and plume models. *J. Geophys. Res.* **80**, 705–717.

WOIDT, W. D. 1978 Finite-element calculations applied to salt-dome analysis. *J. Geophys. Res.* **80**, 705–717.